

Geophysical Research Letters®

RESEARCH LETTER

10.1029/2025GL116894

Key Points:

- Absolute paleointensity experiments conducted on baked sediments constrain geomagnetic dipole strength during the Cretaceous superchron
- Linear Arai diagrams over 60%–90% of the natural remanent magnetization yield a dipole moment of $94.8 \pm 11.0 \text{ ZAm}^2$ from 6 cooling units
- Selected results from volcanic glasses, silicate crystals, and baked sediments reflect a dipole moment 40% stronger than the current value

Supporting Information:

Supporting Information may be found in the online version of this article.

Correspondence to:

F. Lhuillier and J. Meng,
florian.lhuillier@lmu.de;
jmeng@cugb.edu.cn

Citation:

Chi, Y., Lhuillier, F., Meng, J., Zhang, C., & Shcherbakov, V. P. (2025). Geomagnetic dipole strength during the Cretaceous Normal Superchron recorded by baked sediments from Hainan (SE Asia). *Geophysical Research Letters*, 52, e2025GL116894. <https://doi.org/10.1029/2025GL116894>

Received 6 MAY 2025

Accepted 19 AUG 2025

Author Contributions:

Conceptualization: Florian Lhuillier, Jun Meng

Data curation: Yuchen Chi

Formal analysis: Yuchen Chi, Florian Lhuillier

Funding acquisition: Florian Lhuillier, Jun Meng

Methodology: Yuchen Chi

Resources: Jun Meng, Chunyang Zhang

Supervision: Florian Lhuillier

Validation: Florian Lhuillier, Valeriy P. Shcherbakov

Writing – original draft: Florian Lhuillier

Writing – review & editing: Yuchen Chi, Valeriy P. Shcherbakov

© 2025. The Author(s).

This is an open access article under the terms of the [Creative Commons Attribution License](#), which permits use, distribution and reproduction in any medium, provided the original work is properly cited.

Geomagnetic Dipole Strength During the Cretaceous Normal Superchron Recorded by Baked Sediments From Hainan (SE Asia)

Yuchen Chi¹ , Florian Lhuillier¹ , Jun Meng² , Chunyang Zhang², and Valeriy P. Shcherbakov³

¹Department of Earth and Environmental Sciences, Ludwig-Maximilians-Universität, Munich, Germany, ²Frontiers Science Center for Deep-Time Digital Earth, China University of Geosciences (Beijing), Beijing, China, ³Geophysical Observatory Borok, Yaroslavl Oblast, Russia

Abstract The Cretaceous Normal Superchron constitutes an enigmatic ~37-Myr interval of stable polarity in the history of the Earth's magnetic field. The strength of the geomagnetic dipole moment during this interval is controversial, with absolute paleointensity determinations on crystallized volcanic rocks, volcanic glasses, and silicate crystals yielding statistically different averages. In this study, we present the first paleointensities in the mid of the superchron conducted on baked sediments from Hainan (SE Asia). This hitherto underexploited material, akin to baked clays used in archeomagnetism, produces unambiguous linear Arai-Nagata diagrams over 60%–90% of the fraction of natural remanent magnetization. Using strict selection criteria, we show that baked sediments, volcanic glasses, and silicate crystals are consistent with a dipole moment ~40% higher than the present-day value. Relying on 22 independent determinations only, this combined data set leaves open the question of the dependency between geomagnetic dipole strength and reversal frequency.

Plain Language Summary The paleomagnetic field, produced by the convection of liquid iron in the Earth's outer core, regularly switched the polarity of its dipole over geological time and yet experienced an unusual ~37 Myr interval of stable polarity during the Cretaceous. The strength of the paleomagnetic dipole during this so-called superchron remains contentious, with paleointensity experiments yielding values 2–3 times higher for single crystals of silicate than for crystallized volcanic rocks. In this study, we conducted the first absolute paleointensity experiments on sandstones baked by diabase dykes in the mid of the Cretaceous superchron. These baked sediments, similar in their properties to the baked clays used in archeomagnetism, are reliable paleomagnetic recorder, yielding a paleointensity of 40–50 μT at ~105 Ma in Hainan (China). Compared to strictly selected determinations from the absolute paleointensity database, our results from baked sediments are largely consistent with those from silicate crystals and volcanic glasses, pointing to a dipole moment during the Cretaceous superchron ~40% higher than the present-day value. In disagreement with controversial paleointensity determinations conducted on crystallized volcanic rocks, the results from baked sediments, volcanic glasses, and silicate crystals may be consistent with an inverse relationship between geomagnetic dipole strength and reversal frequency.

1. Introduction

The paleomagnetic field, produced by a geodynamo in the Earth's fluid outer core, is schematically characterized by the polarity, variability, and strength of its dipolar component at the Earth's surface (e.g., Merrill et al., 1996). The geomagnetic polarity timescale, interpreted from the marine magnetic anomalies since the Middle Jurassic (e.g., Ogg, 2020), revealed the existence of the Cretaceous Normal Superchron (CNS, 83.65–120.96 Ma)—a ~37 Myr long period of stable polarity, possibly interrupted by short events of reverse polarity (e.g., Zhang et al., 2021). Geodynamo simulations predict more frequent polarity reversals, more pronounced field variability and weaker dipole strength when the convective vigor is increased (e.g., Christensen, 2010; Lhuillier & Gilder, 2013). However, heat flux heterogeneities at the core-mantle boundary (e.g., Frasson et al., 2025) as well as stable stratification in the uppermost core (e.g., Aubert et al., 2025) may also influence the geomagnetic field behavior, questioning the validity of the above prediction for the Earth's dynamo.

The variability of the Earth's magnetic field over centennial to millennial timescales, termed paleosecular variation (PSV), is usually quantified by the dispersion of the virtual geomagnetic poles (VGP scatter S) for a series of volcanic units emplaced at distinct time horizons (e.g., McFadden et al., 1991). Depending on paleolatitude, S is

approximately twice as high at the poles as at the equator during the past 10 Myr (e.g., Cromwell et al., 2018; Tauxe et al., 2024). However, the latitudinal profile of S values during the CNS is statistically indistinguishable from the one during the past 10 Myr (e.g., Doubrovine et al., 2019; Lhuillier et al., 2024). More distinctively, large series of 50–100 volcanics units obtained at 70°–80° paleolatitude revealed an S value 19%–55% lower at the end of the CNS (Lhuillier et al., 2024; Tarduno et al., 2002) than at 66–73 Ma (Lhuillier et al., 2025), the amplitude of the discrepancy depending on the method chosen to filter the transitional directions. Another proxy for PSV, the relative standard deviation in intensity, yielded a value of ~30% during the CNS (Cronin et al., 2001; Lhuillier et al., 2016) compared to 40%–50% during periods with frequent reversals (Eid et al., 2022; Tauxe & Hartl, 1997). Finally, Granot et al. (2012) and Liu et al. (2024) reported enhanced PSV in the middle of the CNS, questioning the existence of a linear relationship between the amplitude of PSV and reversal frequency.

The absolute strength M of the geomagnetic dipole during the CNS is contentious, with reported values ranging from ~10% to ~200% of the present-day value of 80 ZAm² (e.g., Bobrovnikova et al., 2022; Di Chiara et al., 2021; Kulakov et al., 2019). Thellier-style absolute paleointensity (API) experiments, whereby a specimen's natural remanent magnetization (NRM) is progressively replaced by laboratory-induced partial thermoremanent magnetizations (pTRMs), require that the NRM carriers obey the Thellier laws of additivity, reciprocity and independence (e.g., Dunlop, 2011). Violations of these laws may account for the large discrepancies of the API results and typically occur when the NRM grains (a) depart from the single-domain (SD) state (e.g., Kosterov & Prévot, 1998; Xu & Dunlop, 2004), (b) experience magnetostatic interactions (e.g., Coe, 1974; Shcherbakov et al., 1996), (c) carry a thermochemical remanence instead of a pure thermoremanence (e.g., Shcherbakov et al., 2021, 2024), and/or (d) are thermally altered in the course of the experiments. Additionally, uncorrected differences in cooling rate between laboratory and natural conditions may lead to overestimated API determinations (e.g., Biggin et al., 2013; Santos & Tauxe, 2019).

The analysis of the API results during the CNS is particularly complicated since the three major types of materials commonly used for API experiments—oriented paleomagnetic samples of crystallized volcanic rocks (hereinafter “volcanic rocks”), crystals of silicates extracted from igneous rocks (hereinafter “single crystals”), fragments of amorphous volcanic rocks (hereinafter “volcanic glasses”)—yield statistically distinct averages (e.g., Bobrovnikova et al., 2022; Ingham et al., 2014). Volcanic rocks, which may be more prone to alteration and contamination by multidomain remanence carriers (e.g., Cottrell & Tarduno, 2000), yield the lowest estimates of M up to ~10% of the present-day value (e.g., Shcherbakova et al., 2012; Zhu et al., 2008). Single crystals and volcanic glasses specifically target SD remanence carriers, at the expense of losing the possibility to determine the associated paleodirections and amplifying anisotropy effects. Single crystals of millimetric size approach the limits for which the Maxwell-Boltzmann statistics can be applied (e.g., Berndt et al., 2016) and yield the highest estimates of M up to ~200% of the present-day value (e.g., Tarduno et al., 2001, 2002). Volcanic glasses may partially melt in the course of the API experiments (e.g., Smirnov & Tarduno, 2003) and yield dispersion twice as high as for other materials (e.g., Di Chiara et al., 2021; Tauxe & Staudigel, 2004).

By analogy with the baked clays used in archeomagnetism (e.g., Thellier & Thellier, 1959), sediments baked by intrusions or lavas usually contain ideal remanence carriers which are well suited for API determinations (e.g., Meng et al., 2020). We present in this letter the first API results on baked sediments characterizing the state of the geodynamo in the middle of the CNS. To this end, we focus on a swarm of diabase dykes intruding fine-grained sandstones from the Lumuwan Formation in the prefecture of Qionghai in Hainan (China, Figures 1a and 1b).

2. Materials and Methods

2.1. Geological and Paleomagnetic Setting

Meng et al. (2022) investigated the paleomagnetism of eight dykes from the Shangling quarry (19.1159°N, 110.3644°E) and produced four profiles in the host sandstones to determine the influence of baking on the magnetization of the sediments. Carried by low-Ti titanomagnetite, the remanence of the dykes yielded a negative fold test, indicating that the dykes were intruded after the sediments were folded. According to thermal demagnetization spectra, the remanence of the unbaked sediments was dominantly carried by hematite whereas the remanence of the baked sediments was dominantly carried by magnetite. The reduction of hematite to magnetite being unlikely in the absence of organic material during the intrusion of the dykes, fine magnetite grains were likely exsolved within silicate crystals during the baking of the sediments above 600°C (e.g., Davis, 1981; Tarduno et al., 2006). In a distance less than 5 cm from the dyke, the paleodirection of the sediments

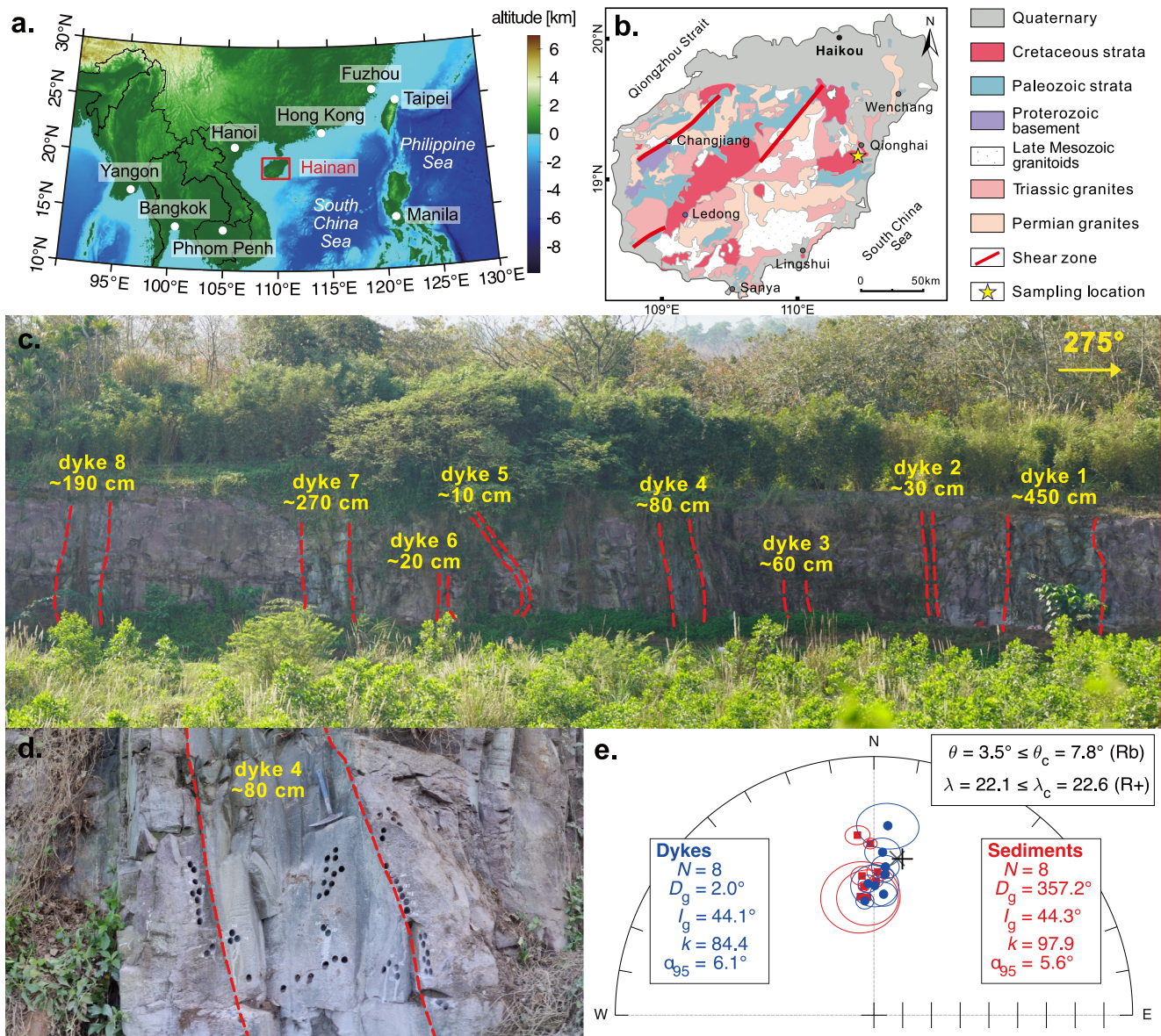


Figure 1. Geological and paleomagnetic setting. (a) Overview topographic map of the northern part of SE Asia showing the location of the Hainan Island. (b) Geological map of Hainan showing the location of the Shangling quarry investigated in this study. (c) Field photograph showing the eight diabase dykes sampled in 2023. (d) Enlargement of site 4 showing the sampled baked sediments at the dyke's margin. (e) Comparison of the mean paleodirections (D_g, I_g) obtained from the dyke (blue disks) and the baked sediments (red squares). The parameters k and α_{95} represent Fisher (1953)'s precision parameter and the 95% confidence radius. The inset provides the results of the common-mean tests of McFadden and McElhinny (1990) and Heslop et al. (2023).

was indistinguishable from the one of the dyke, supporting the pristine nature of the remanence of the dykes. Nine magmatic zircons picked from those dykes yielded a $^{206}\text{Pb}/^{238}\text{U}$ age of 104.6 ± 0.7 Ma (Meng et al., 2022), consistent with the less precise U-Pb SHRIMP age of 101 ± 4 Ma for the same dyke system (Dilek & Tang, 2021).

In addition to the 101 baked sediments from Meng et al. (2022) sampled in 2021, we drilled 242 paleomagnetic cores (186 for baked sediments and 56 for the diabase dykes) in 2023 (Figures 1c and 1d; see also Figure S1 in Supporting Information S1). We successfully sampled seven of the eight sites (each site consisting of the diabase dyke and the associated baked sandstones) shown in Figure 1c, with sites 1, 2, and 4 corresponding to sites 1B, 1A, and 5 from Meng et al. (2022); site 7 was not suitable for paleomagnetic sampling. Additionally, we analyzed site 2 from Meng et al. (2022) that was not accessible anymore in 2023; it is termed site 9 in this study. The

sediments from 2023 were drilled at 1–9 cm (median of 2.5 cm) from the dyke; those from 2021, initially not intended for API experiments, at 2–172 cm (median of 10 cm) from the dyke.

2.2. Absolute Paleointensity Experiments

To determine estimates of the ancient field B_{anc} , we conducted Thellier-style experiments (Thellier & Thellier, 1959) on 8.8-mm diameter cores (182 from baked sediments and 48 from diabase dykes) using an ASC TD48 double-chamber furnace and an AGICO JR6 spinner magnetometer in the magnetically shielded room of the Ludwig-Maximilians-Universität München. In the course of the stepwise replacement of a specimen's NRM by a laboratory-induced pTRM (in 11–12 temperature steps, in a controlled field B_{lab} of 40 or 50 μT), we intercalated pTRM checks to detect thermal alteration (Coe, 1967) and pTRM tail checks to detect non-ideal remanence carriers violating the pTRM reciprocity law (Riisager & Riisager, 2001). We determined B_{anc} as the slope of the linear segment multiplied by B_{lab} in the Arai-Nagata diagram (Nagata et al., 1963). For our final estimates, we averaged, first at the sample level, then at the site level, the most robust API determinations selected using improved PICRIT-03 criteria (Kissel & Laj, 2004), where the threshold for the NRM fraction f was raised from 0.35 to 0.70.

2.3. Paleomagnetic and Rock-Magnetic Experiments

We determined the paleodirections of the diabase samples by alternating field demagnetization using the automated SushiBar system (Wack & Gilder, 2012) whereas those of the baked sediments were recovered from the Thellier-Coe experiments. To characterize the nature and thermostability of the remanence carriers, we conducted hysteresis loops on select samples using a LakeShore MicroMag 3900 vibrating sample magnetometer as well as thermomagnetic curves of the saturation magnetization using a custom-made Curie balance. On four characteristic samples, we performed scanning electron microscopy (SEM) of polished sections using a TESCAN VEGA II LMU device and X-ray diffractometry (XRD) of magnetic separates using a STOE STADI MP device.

2.4. Absolute Paleointensity Database

Following Bobrovnikova et al. (2022), we focused on the Thellier-style determinations with pTRM checks available during the Cretaceous period (66.0–143.1 Ma). For this time interval, two studies (Alva-Valdivia et al., 2023; Zhu et al., 2002) were added to the Borok-Munich database (Eid et al., 2022), for a total of 302 records from 60 studies. For the selection, we employed the simple criteria of Perrin and Shcherbakov (1997) in terms of the number of determinations per cooling unit (N_{int}) and the within-unit relative standard error (RSE).

3. Experimental Results

For the eight investigated sites, we first checked the consistency between the paleodirections of the dykes and those of the baked sediments. Considering the eight sites separately (Figure S2 in Supporting Information S1), the baked contact test is positive for six of them; negative for sites 1 and 4 despite a critical angle θ between the means of the two populations not exceeding 5° . Considering the eight sites together (Figure 1e), the baked contact test is positive, with $\theta = 3.5^\circ \leq \theta_c = 7.8^\circ$ for the conventional common-mean test of McFadden and McElhinny (1990) and $\lambda = 22.1 \leq \lambda_c = 22.6$ for the bootstrap common-mean test of Heslop et al. (2023).

None of the Thellier experiments on the diabase dykes could be interpreted due to erratic and/or convex-shaped Arai-Nagata diagram. Focusing on the baked sediments, we successfully interpreted 10 samples or more for sites 1, 2, 3, 4, and 9; three to five samples for sites 5 and 6; none of them for site 8 (Table 1). The samples from sites 2–4 are mainly characterized by one-sloped Arai-Nagata diagrams over 60%–90% of the NRM fraction (Figures 2a–2c and Figures S3c–S3h in Supporting Information S1). In contrast, the samples from sites 1, 5, 6, and 9 often show two-sloped and/or convex-shaped Arai-Nagata diagrams, as a consequence of the insufficient baking of the sediments (distance greater than 5 cm from the dyke's margin) and/or of the presence of non-ideal remanence carriers (Figure 2d, Figures S3a, S3b, and S4 in Supporting Information S1). To exclude these ambiguous determinations, we applied modified PICRIT-03 selection criteria to our API results (see Section 2.3). This allowed us to significantly reduce by a factor of 6–7 the dispersion about the mean for sites 1, 2, and 9; more moderately by a factor of 1.3 for the other sites (Figure S5 in Supporting Information S1). At the end of this selection process, sites 2–4 are ranked as excellent with eight samples or more used to compute the averages; sites 1, 6, and 9 are of intermediate quality with $N_{\text{int}} = 1$ –4; site 5 is rejected with $N_{\text{int}} = 0$ (Table 1). The obtained estimates B_{anc} of the

Table 1
Site-Mean Paleodirections and Paleointensities

Site	N_{int}	N_{int}^1	N_{int}^0	B_{anc}	$\sigma(B_{\text{anc}})$	VDM	N_{dir}	N_{dir}^0	D_g	I_g	k	α_{95}
1/1B (2021)	4	28	39	42.0	1.2	84.0 (68.9)	23	40	0.9	47.0	225.3	2.0
2/1A (2021)	10	22	34	41.3	1.1	93.4 (86.9)	19	37	358.8	34.0	311.8	1.9
3	8	14	18	39.8	4.4	82.4 (74.2)	12	18	1.5	43.9	191.6	3.1
4/5 (2021)	14	20	20	52.5	3.9	103.2 (91.8)	19	23	355.5	48.7	417.5	1.6
5	0	3	16				6	16	353.4	52.0	33.2	11.8
6	1	5	16	50.4		94.8 (89.1)	9	16	356.9	52.3	32.3	9.2
8	0	0	7				7	7	354.8	30.8	315.1	3.4
9/2 (2021)	2	13	20	54.3	1.3	111.0 (98.8)	11	20	355.1	45.1	201.8	3.2

Note. The quantity B_{anc} is the site-mean API in μT determined from N_{int} individual samples passing our selection criteria, together with its relative standard deviation $\sigma(B_{\text{anc}})$ and the virtual dipole moment (VDM) in ZAm^2 . The parenthesized values are corrected for cooling rate using the predictions of Table S3 in Supporting Information S1. The quantity N_{int}^0 (resp. N_{int}^1) is the number of measured (resp. interpreted) samples for each site. The quantities (D_g, I_g) represent the site-mean paleodirection in degrees determined from N_{dir} individual samples, together with its precision parameter k and the 95% confidence radius α_{95} . The quantity N_{dir}^0 is the number of measured samples for each site.

ancient field range from ~ 40 to $55 \mu\text{T}$, which amounts to virtual dipole moment (VDM) values from ~ 80 to 110ZAm^2 . Note that our VDM values for sites 2–4 agree to within 3% with the averages calculated using the CCRIT selection criteria (see Table S1 in Supporting Information S1, Tauxe et al., 2016).

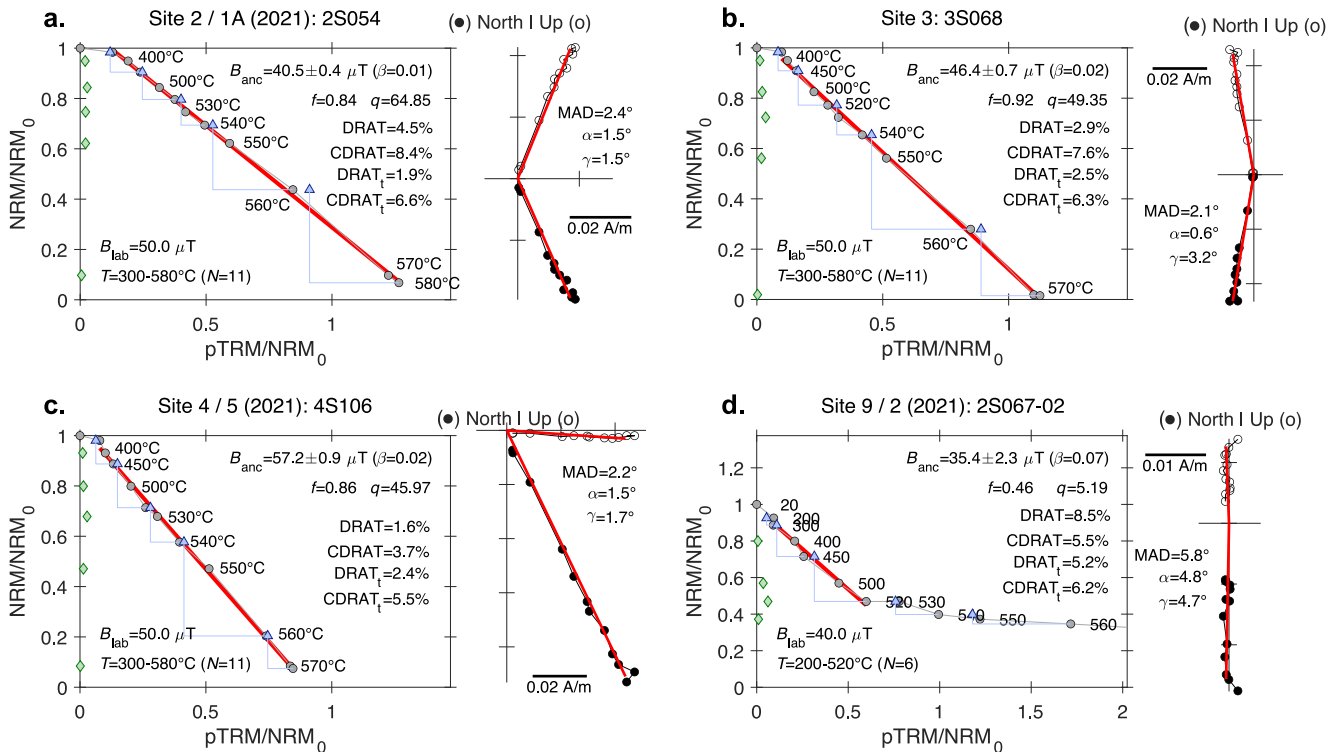


Figure 2. Examples of Arai-Nagata diagrams, showing in red the fitted line over the temperature segment T ; B_{anc} is the ancient field estimate, β the relative standard error, f the fraction of natural remanent magnetization (NRM), q the quality factor (Coe et al., 1978). Blue triangle (green diamonds) show the partial thermoremanent magnetization (pTRM) checks (pTRM tail checks) where DRAT (DRAT_t) is the maximum difference ratio measured from the pTRM checks (pTRM tail checks) according to Selkin and Tauxe (2000); CDRAT (CDRAT_t) is the absolute value of the sum of the pTRM checks (pTRM tail checks) differences according to Kissel and Laj (2004). Vector endpoint diagrams of the NRM in course of the Thellier-Coe experiments are provided in core coordinates to the right of the Arai-Nagata diagrams, where MAD is the maximum angular deviation, α is the angle between origin-anchored and free-floating fitted directions, and γ is the angle between the measured pTRM direction and the applied field direction.

In terms of rock-magnetic properties, the hysteresis loops of the eight sites are characterized by large values of the coercivity B_C ranging from ~ 25 to 225 mT (Figures S6 and S7 in Supporting Information S1). We could not identify any relationship between B_{anc} and B_C . For instance, site 2 with $B_C = 200\text{--}225$ mT yields the same B_{anc} as site 3 with $B_C = 25\text{--}50$ mT. Likewise, we could not anticipate the failure of the Thellier-Coe experiments for sites 5 and 8 from the inspection of the hysteresis properties. The thermomagnetic curves in saturation magnetization M_S are consistent with the presence of both magnetite and hematite phases (Figure S6 in Supporting Information S1). They also reveal high thermostability up to $600^\circ\text{C}\text{--}700^\circ\text{C}$, except for sample 1S034 from site 1 that is only stable up to 600°C . For this latter sample, the cooling branch of the $M_S(T)$ curve shows the formation of magnetite above 600°C . SEM indicates the presence of oxy-exsolved magnetite (Figure S8 in Supporting Information S1). XRD confirms the coexistence of magnetite and hematite for site 1 (Table S2 in Supporting Information S1). Conversely, XRD fails to detect magnetite for sites 2 and 4 but detect 30%–60% of quartz in the magnetic separates. We speculate that fine-grained magnetite is concealed in the silicate crystals (e.g., Eliseev et al., 2022), consistent with the idea that magnetite was exsolved during the baking of the sediments (e.g., Davis, 1981; Tarduno et al., 2006).

4. Geomagnetic Dipole Strength During the CNS

In the absence of selection on the Thellier-type determinations from the API database (Figure 3a), the average dipole moment during the CNS for the volcanic rocks ($M = 45.2 \pm 19.1 \text{ ZAm}^2$, $N = 88$), volcanic glasses ($M = 69.1 \pm 41.1 \text{ ZAm}^2$, $N = 58$), baked sediments ($M = 94.8 \pm 11.0 \text{ ZAm}^2$, $N = 6$), and single crystals ($M = 124.1 \pm 11.7 \text{ ZAm}^2$, $N = 16$) are statistically distinct when compared pairwise using a two-sample Kolmogorov-Smirnov test (p -value from 10^{-3} to 10^{-13}). This observation points to the presence of biased API records that could not be fully removed by specimen-level selection criteria (e.g., Kissel & Laj, 2004; Paterson et al., 2014). When lenient selection criteria are applied to the API database ($N \geq 5$, $\text{RSE} \leq 10\%$, Figure 3b), the average moments for the volcanic rocks ($M = 43.7 \pm 17.0 \text{ ZAm}^2$, $N = 39$) and single crystals ($M = 123.0 \pm 11.3 \text{ ZAm}^2$, $N = 15$) remain distinct (p -value of 10^{-10}), whereas our determinations on baked sediments from sites 2–4 ($M = 93.0 \pm 10.4 \text{ ZAm}^2$, $N = 3$) become indistinguishable from those on volcanic glasses ($M = 82.0 \pm 39.6 \text{ ZAm}^2$, $N = 17$; p -value of 0.2). When stricter selection criteria are considered ($N \geq 5$, $\text{RSE} \leq 5\%$, Figure 3c), the average moment for the volcanic rocks ($M = 45.1 \pm 15.8 \text{ ZAm}^2$, $N = 26$), $\sim 45\%$ lower than the present-day value, persistently remains distinct from the averages of the other data sets (p -value from 10^{-3} to 10^{-8}). In contrast, the averages for the single crystals ($M = 122.7 \pm 12.9 \text{ ZAm}^2$, $N = 11$), volcanic glasses ($M = 106.5 \pm 35.7 \text{ ZAm}^2$, $N = 8$) and baked sediments ($M = 93.0 \pm 10.4 \text{ ZAm}^2$, $N = 3$) coincide more closely (p -values from 0.01 to 0.5). The average of these three data sets ($M = 112.8 \pm 25.2 \text{ ZAm}^2$, $N = 22$) points to a dipole moment $\sim 40\%$ stronger than the present-day value, consistent with the conclusions by Tarduno et al. (2001, 2002). This average would also be $\sim 50\%$ higher than the average for the Cretaceous without the CNS ($M = 75.7 \pm 20.5 \text{ ZAm}^2$, $N = 4$). Note that this latter value is only constrained by two determinations on volcanic glasses (Juárez et al., 1998; Selkin & Tauxe, 2000) and two determinations on baked sediments (Meng et al., 2020) from the Late Cretaceous (Figure 3c), leading to higher dispersion when strict selection criteria are applied. Generally, the previous analysis in terms of average dipole moment relies on the assumption that the state of the geodynamo was stationary during the CNS and the discrepancies in the API results are due to experimental errors. Nevertheless, we cannot exclude that the observed variability in the API results is also partly due to temporal changes of the geodynamo during the CNS, as suggested by Granot et al. (2012) from the analysis of sea-floor magnetic anomalies. More API determinations passing stringent reliability criteria are needed to discriminate between these two scenarios.

Although marginally considered in the records of the API database, differences in cooling rate between laboratory and natural conditions may bias API determinations on SD grain (e.g., Dodson & McClelland-Brown, 1980; Halgedahl et al., 1980). To quantify this effect on our 39 selected specimens, we successively applied three TRMs by cooling the specimens from 580°C to room temperature in a laboratory field of $45 \mu\text{T}$: TRM₁ with a cooling time λ_{TRM_1} of 1 hr, TRM₂ with a cooling time λ_{TRM_2} of 12 hr, and TRM₃ with a cooling time λ_{TRM_3} of 1 hr. We observed that the alteration ratio $r_2 = (\text{TRM}_3 - \text{TRM}_1)/\text{TRM}_1$ linearly increased with the cooling-rate ratio $r_1 = (\text{TRM}_2 - \text{TRM}_1)/\text{TRM}_1$, with a slope of ~ 1 and a y -intercept of -0.1 (Figure S9a in Supporting Information S1). This indicates that our specimens were not thermally stable at 580°C . Assume $\text{TRM}_2 = \text{TRM}_1 + \delta\text{TRM}_1 + \delta\text{TRM}_2$, where δTRM_1 (resp. δTRM_2) is the magnetization excess acquired due to mineralogical changes (resp. the cooling-rate effect). Assume now that the samples have been stabilized

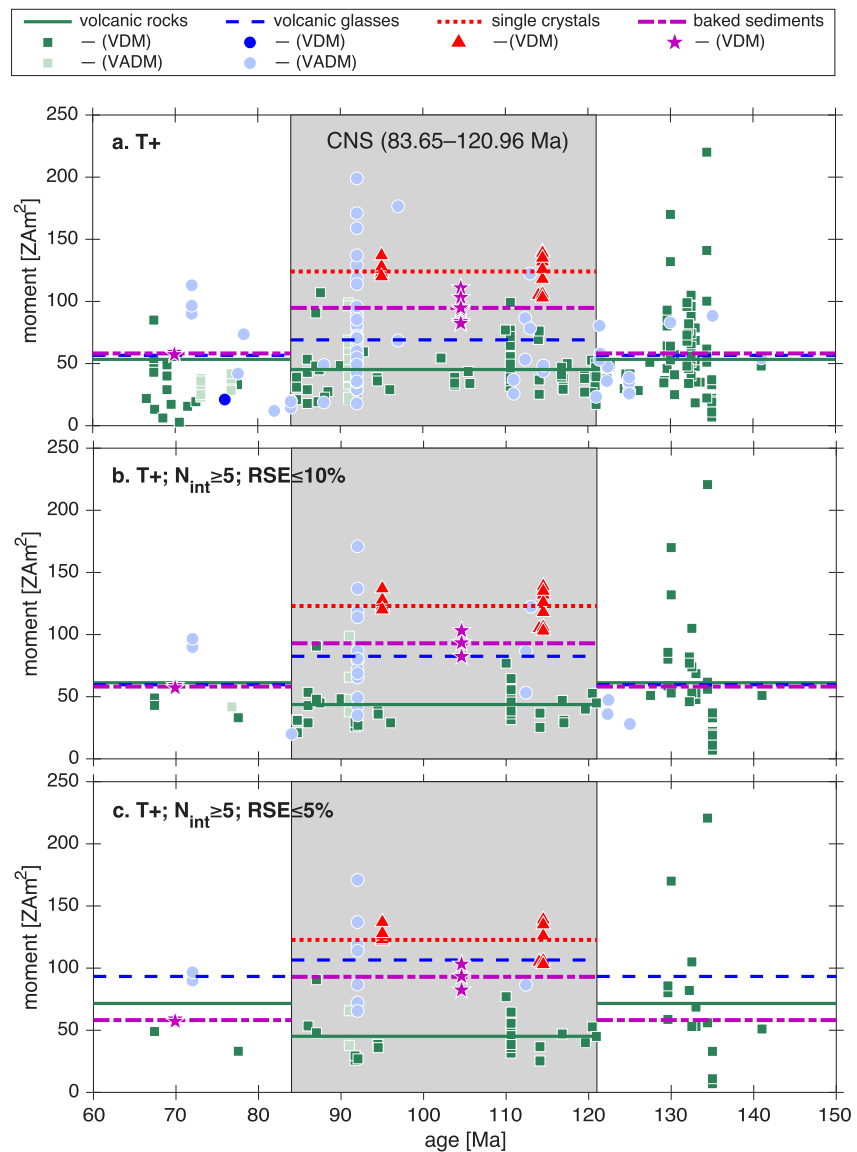


Figure 3. Analysis of the Thellier-style determinations from the absolute paleointensity database. (a–c) Time evolution of the reconstructed dipole strength (virtual dipole moment; or virtual axis dipole moment during the Cretaceous for different types of material—volcanic rocks (green squares), volcanic glasses (blue disks), single crystals (red triangle), and baked sediments (purple stars)—and selection criteria in terms of the number of determinations per cooling unit (N_{int}) and the within-unit relative standard error. The horizontal lines show the averages during Cretaceous Normal Superchron (CNS), or during the Cretaceous without the CNS.

during the acquisition of TRM_2 , we then obtain $TRM_3 = TRM_1 + \delta TRM_1$ and the relative increase $\delta TRM_2/ TRM_1$ in magnetization due to the cooling-rate effect equates $r_1 - r_2 = 0.1$. This value largely agrees with the theoretical works on SD grains, which predict $q = \log_{10}(\lambda_{TRM_2}/\lambda_{TRM_1})$ on the order of 1.3–1.7 for $\delta TRM_2/ TRM_1 = 0.1$ (see Figure 5b of Shcherbakov et al., 2021). On the one hand, the observation of a cooling-rate dependency in our baked sediments indirectly proves that our remanence carriers are SD-like. On the other hand, it underlines the necessity to conduct a cooling-rate correction. Assuming a magma temperature of 1,100°C and a thermal diffusivity of 1.15 mm²/s for baked sandstones, we predict cooling times to reach the blocking temperature of 300°C varying from 13 to 4,400 hr depending on the dyke's thickness (Table S3 and Figure S9b in Supporting Information S1, Jaeger, 1964). Assuming that the NRM/TRM ratio is overestimated by ~5% for a tenfold increase in the cooling rate (e.g., Shcherbakov et al., 2021), our API estimates may be overestimated by 6%–18% (Table S3 in Supporting Information S1). Should these predictions be correct, our

VDM values obtained from baked sediments would range from 69 to 100 ZAm² (84–111 ZAm² before correction) and not significantly differ from the present-day value.

5. Conclusions

Hitherto little explored baked sediments, similar to the bricks and potteries studied by Thellier and Thellier (1959), present some advantages—SD-like magnetic grains carrying a pure TRM, possibility to conduct a baked contact test to assess the pristine nature of the NRM—for the determination of absolute paleointensities. The Hainan sandstones baked by diabase dykes during the CNS provide unambiguous single-sloped Arai-Nagata diagrams, as a likely result of a pure thermoremanent magnetization carried by fine-grained magnetite. When strict selection criteria are applied to the API database, our results become statistically indistinguishable from those determined on volcanic glasses and single crystals. The concordance of the results obtained from these three types of material suggests that a strong dipole moment (~40% higher than the present-day value) is more likely to describe the state of the geodynamo during the CNS than the determinations from volcanic rocks pointing to a weak dipole moment (~45% lower than the present-day value). This being said, the number of API determinations from volcanic glasses, single crystals and baked sediments passing stringent reliability criteria is still insufficient to draw definitive conclusions about the average state and variability of the geodynamo during the CNS.

Data Availability Statement

The raw paleomagnetic data are available in the MagIC database (Chi et al., 2025). The Borok-Munich absolute paleointensity database is available on Open Data LMU (Lhuillier, 2022).

Acknowledgments

This project was funded by the National Science and Technology Major Project of China—Grants 2024ZD1001105 and 2024ZD1000601—and the Sino-German Center for Research Promotion (SGC)—Grant 1681. Y.C. acknowledges the support by the China Scholarship Council (CSC)—Grant 202208080269. F.L. acknowledges the support by the German Research Foundation (DFG)—Grant 521315821. J.M. acknowledges the support by the Scientific Research Innovation Capability Support Project for Young Faculty—Grant ZYGXQNJSKYCXNLZCXM-PIP—and the National Natural Science Foundation of China—Grants 42322402 and 42488201. The XRD experiments and interpretation of the rock-magnetic data were supported by the Russian Science Foundation (RSF)—Grant 23-17-00112 (V.P.S.). We thank Zihao Wang, Yanan Zhao, and Zhaoyang Zhou for their help during the 2021 field campaign; Tao Yu, Chenyu Li, and Ningtao Li for their help during the 2023 field campaign. We thank Monika Korte for editorial handling; Lisa Tauxe and an anonymous referee for their constructive reviews. Open Access funding enabled and organized by Projekt DEAL.

References

- Alva-Valdivia, L. M., Savian, J. F., Tomé, C. R., Hernández-Cardona, A., Tolotti, C. D. K., Gomes, M. E. B., & González-Rangel, J. A. (2023). Full vector paleomagnetic estimation from the Paraná-Etendeka Large Igneous Province, southern Brazil: Implications on the onset of Cretaceous Normal Superchron. *Physics of the Earth and Planetary Interiors*, 343, 107088. <https://doi.org/10.1016/j.pepi.2023.107088>
- Aubert, J., Landeau, M., Fournier, A., & Gastine, T. (2025). Core-surface kinematic control of polarity reversals in advanced geodynamo simulations. *Physics of the Earth and Planetary Interiors*, 364, 107365. <https://doi.org/10.1016/j.pepi.2025.107365>
- Berndt, T., Muxworthy, A. R., & Fabian, K. (2016). Does size matter? Statistical limits of paleomagnetic field reconstruction from small rock specimens. *Journal of Geophysical Research: Solid Earth*, 121(1), 15–26. <https://doi.org/10.1002/2015jb012441>
- Biggin, A. J., Badojo, S., Hodgson, E., Muxworthy, A. R., Shaw, J., & Dekkers, M. J. (2013). The effect of cooling rate on the intensity of thermoremanent magnetization (TRM) acquired by assemblages of pseudo-single domain, multidomain and interacting single-domain grains. *Geophysical Journal International*, 193(3), 1239–1249. <https://doi.org/10.1093/gji/ggt078>
- Bobrovnikova, E. M., Lhuillier, F., Shcherbakov, V. P., Shcherbakova, V. V., Zhidkov, G. V., Lebedev, I. E., et al. (2022). High-latitude paleointensities during the Cretaceous normal superchron from the Okhotsk-Chukotka volcanic belt. *Journal of Geophysical Research: Solid Earth*, 127(2), e2021JB023551. <https://doi.org/10.1029/2021jb023551>
- Chi, Y., Lhuillier, F., Meng, J., Zhang, C., & Shcherbakov, V. P. (2025). Geomagnetic dipole strength during the Cretaceous normal superchron recorded by baked sediments from Hainan (SE Asia) [Dataset]. *Magnetics Information Consortium*. <https://doi.org/10.7288/V4/MAGIC/20385>
- Christensen, U. R. (2010). Dynamo scaling laws and applications to the planets. *Space Science Reviews*, 152(1–4), 565–590. <https://doi.org/10.1007/s11214-009-9553-2>
- Coe, R. S. (1967). The determination of paleo-intensities of the Earth's magnetic field with emphasis on mechanisms which could cause non-ideal behavior in Thellier's method. *Journal of Geomagnetism and Geoelectricity*, 19(3), 157–179. <https://doi.org/10.5636/jgg.19.157>
- Coe, R. S. (1974). The effect of magnetic interactions on paleointensity determinations by the Thelliers' method. *Journal of Geomagnetism and Geoelectricity*, 26(3), 311–317. <https://doi.org/10.5636/jgg.26.311>
- Coe, R. S., Grommé, C. S., & Mankinen, E. A. (1978). Geomagnetic paleointensities from radiocarbon-dated lava flows on Hawaii and the question of the Pacific nondipole low. *Journal of Geophysical Research*, 83(B4), 1740–1756. <https://doi.org/10.1029/JB083iB04p01740>
- Cottrell, R. D., & Tarduno, J. A. (2000). In search of high-fidelity geomagnetic paleointensities: A comparison of single plagioclase crystal and whole rock Thellier-Thellier analyses. *Journal of Geophysical Research*, 105(B10), 23579–23594. <https://doi.org/10.1029/2000JB900219>
- Cromwell, G., Johnson, C. L., Tauxe, L., Constable, C. G., & Jarboe, N. A. (2018). PSV10: A global data set for 0–10 Ma time-averaged field and paleosecular variation studies. *Geochemistry, Geophysics, Geosystems*, 57(9), 1533–1558. <https://doi.org/10.1002/2017GC007318>
- Cronin, M., Tauxe, L., Constable, C. G., Selkin, P. A., & Pick, T. (2001). Noise in the quiet zone. *Earth and Planetary Science Letters*, 190(1–2), 13–30. [https://doi.org/10.1016/S0012-821X\(01\)00354-5](https://doi.org/10.1016/S0012-821X(01)00354-5)
- Davis, K. E. (1981). Magnetite rods in plagioclase as the primary carrier of stable NRM in ocean floor Gabbros. *Earth and Planetary Science Letters*, 55(1), 190–198. [https://doi.org/10.1016/0012-821X\(81\)90098-4](https://doi.org/10.1016/0012-821X(81)90098-4)
- Di Chiara, A., Tauxe, L., Staudigel, H., Florindo, F., Protti, M., Yu, Y., et al. (2021). Earth's magnetic field strength and the Cretaceous normal superchron: New data from Costa Rica. *Geochemistry, Geophysics, Geosystems*, 22(4), e2020GC009605. <https://doi.org/10.1029/2020gc009605>
- Dilek, Y., & Tang, L. (2021). Magmatic record of the Mesozoic geology of Hainan Island and its implications for the Mesozoic tectonomagmatic evolution of SE China: Effects of slab geometry and dynamics in continental tectonics. *Geological Magazine*, 158(1), 118–142. <https://doi.org/10.1017/S0016756820001211>
- Dodson, M. H., & McClelland-Brown, E. (1980). Magnetic blocking temperatures of single-domain grains during slow cooling. *Journal of Geophysical Research*, 85(B5), 2625–2637. <https://doi.org/10.1029/JB085iB05p02625>

- Dobrovine, P. V., Veikkolainen, T., Pesonen, L. J., Piispa, E., Ots, S., Smirnov, A. V., et al. (2019). Latitude dependence of geomagnetic paleosecular variation and its relation to the frequency of magnetic reversals: Observations from the Cretaceous and Jurassic. *Geochemistry, Geophysics, Geosystems*, 20(3), 1240–1279. <https://doi.org/10.1029/2018GC007863>
- Dunlop, D. J. (2011). Physical basis of the Thellier–Thellier and related paleointensity methods. *Earth and Planetary Science Letters*, 187(3–4), 118–138. <https://doi.org/10.1016/j.pepi.2011.03.006>
- Eid, B., Lhuillier, F., Shcherbakov, V. P., & Shcherbakova, V. V. (2022). Do changes in geomagnetic secular variation, dipole moment and polarity reversal frequency correlate over the past 155 Myr? *Geophysical Journal International*, 230(2), 1132–1146. <https://doi.org/10.1093/gji/ggac112>
- Eliseev, A. A., Shcherbakova, V. V., Metelkin, D. V., Mikhaltsov, N. E., Zhidkov, G. V., Abashev, V. V., & Rogov, A. M. (2022). Low geomagnetic field paleointensity on the Permian–Triassic boundary from study of the Kuznetsk basin traps (southern Siberia). *Russian Geology and Geophysics*, 63(2), 193–207. <https://doi.org/10.2113/rgg20204330>
- Fisher, R. (1953). Dispersion on a sphere. *Proceedings of the Royal Society of London Series A*, 217(1130), 295–305. <https://doi.org/10.1098/rspa.1953.0064>
- Frasson, T., Schaeffer, N., Nataf, H. C., & Labrosse, S. (2025). Geomagnetic dipole stability and zonal flows controlled by mantle heat flux heterogeneities. *Geophysical Journal International*, 240(3), 1481–1504. <https://doi.org/10.1093/gji/ggae457>
- Granot, R., Dymet, J., & Gallet, Y. (2012). Geomagnetic field variability during the Cretaceous normal superchron. *Nature Geoscience*, 5(3), 220–223. <https://doi.org/10.1038/ngeo1404>
- Halgedahl, S. L., Day, R., & Fuller, M. D. (1980). The effect of cooling rate on the intensity of weak-field TRM in single-domain magnetite. *Journal of Geophysical Research*, 85(B7), 3690–3698. <https://doi.org/10.1029/JB085iB07p03690>
- Heslop, D., Sealey, J. L., Wood, A. T. A., Tauxe, L., & Roberts, A. P. (2023). A bootstrap common mean direction test. *Journal of Geophysical Research: Solid Earth*, 128(8), e2023JB026983. <https://doi.org/10.1029/2023jb026983>
- Ingham, E., Heslop, D., Roberts, A. P., Hawkins, R., & Sambridge, M. (2014). Is there a link between geomagnetic reversal frequency and paleointensity? A Bayesian approach. *Journal of Geophysical Research: Solid Earth*, 119(7), 5290–5304. <https://doi.org/10.1002/2014JB010947>
- Jaeger, J. C. (1964). Thermal effects of intrusions. *Reviews of Geophysics*, 2(3), 443–466. <https://doi.org/10.1029/RG002i003p00443>
- Juárez, M. T., Tauxe, L., Gee, J. S., & Pick, T. (1998). The intensity of the Earth's magnetic field over the past 160 million years. *Nature*, 394(6696), 878–881. <https://doi.org/10.1038/29746>
- Kissel, C., & Laj, C. (2004). Improvements in procedure and paleointensity selection criteria (PICRIT-03) for Thellier and Thellier determinations: Application to Hawaiian basaltic long cores. *Physics of the Earth and Planetary Interiors*, 147(2–3), 155–169. <https://doi.org/10.1016/j.pepi.2004.06.010>
- Kosterov, A. A., & Prévot, M. (1998). Possible mechanisms causing failure of Thellier paleointensity experiments in some basalts. *Geophysical Journal International*, 134(2), 554–572. <https://doi.org/10.1046/j.1365-246x.1998.00581.x>
- Kulakov, E. V., Sprain, C. J., Dobrovine, P. V., Smirnov, A. V., Paterson, G. A., Hawkins, L., et al. (2019). Analysis of an updated paleointensity database (Q_{PI} -PINT) for 65–200 Ma: Implications for the long-term history of dipole moment through the Mesozoic. *Journal of Geophysical Research: Solid Earth*, 124(10), 9999–10022. <https://doi.org/10.1029/2018JB017287>
- Lhuillier, F. (2022). Borok-munich absolute paleointensity database [Dataset]. *Open Data LMU*. <https://doi.org/10.5282/ubm/data.612>
- Lhuillier, F., & Gilder, S. A. (2013). Quantifying paleosecular variation: Insights from numerical dynamo simulations. *Earth and Planetary Science Letters*, 382, 87–97. <https://doi.org/10.1016/j.epsl.2013.08.048>
- Lhuillier, F., Gilder, S. A., Wack, M., He, K., Petersen, N., Singer, B. S., et al. (2016). More stable yet bimodal geodynamo during the Cretaceous superchron? *Geophysical Research Letters*, 43(12), 6170–6177. <https://doi.org/10.1002/2016GL069303>
- Lhuillier, F., Lebedev, I. E., Tikhomirov, P. L., & Pavlov, V. E. (2024). High-Latitude geomagnetic secular variation at the end of the Cretaceous normal superchron recorded by volcanic flows from the Okhotsk-Chukotka volcanic belt. *Journal of Geophysical Research: Solid Earth*, 129(1), e2023JB027550. <https://doi.org/10.1029/2023jb027550>
- Lhuillier, F., Lebedev, I. E., Tikhomirov, P. L., & Pavlov, V. E. (2025). Is the geodynamo characterized by a distinct geomagnetic secular variation regime during the Cretaceous normal superchron? *Journal of Geophysical Research: Solid Earth*, 130(4), e2024JB030928. <https://doi.org/10.1029/2024jb030928>
- Liu, X., Li, Y. X., & Richter, C. (2024). Salient changes of Earth's magnetic field toward the end of Cretaceous normal superchron (CNS). *Journal of Geophysical Research: Solid Earth*, 129(4), e2023JB028104. <https://doi.org/10.1029/2023jb028104>
- McFadden, P. L., & McElhinny, M. W. (1990). Classification of the reversal test in palaeomagnetism. *Geophysical Journal International*, 103(3), 725–729. <https://doi.org/10.1111/j.1365-246X.1990.tb05683.x>
- McFadden, P. L., Merrill, R. T., McElhinny, M. W., & Lee, S. (1991). Reversals of the Earth's magnetic field and temporal variations of the dynamo families. *Journal of Geophysical Research*, 96(B3), 3923–3933. <https://doi.org/10.1029/90JB02275>
- Meng, J., Gilder, S. A., Li, Y., Chen, Y., Zhang, C., Zhou, Z., et al. (2022). Remagnetization age and mechanism of Cretaceous sediments in relation to dyke intrusion, Hainan Island: Tectonic implications for south China and the red river fault. *Journal of Geophysical Research: Solid Earth*, 127(1), e2021JB023474. <https://doi.org/10.1029/2021jb023474>
- Meng, J., Lhuillier, F., Wang, C., Liu, H., Eid, B., & Li, Y. (2020). Paleomagnetism of Paleocene-Maastrichtian (60–70 Ma) lava flows from Tian Shan (Central Asia): Directional analysis and paleointensities. *Journal of Geophysical Research: Solid Earth*, 125(9), e2019JB018631. <https://doi.org/10.1029/2019JB018631>
- Merrill, R. T., McElhinny, M. W., & McFadden, P. L. (1996). *The magnetic field of the Earth: Paleomagnetism, the core, and the deep mantle* (2nd ed., Vol. 63). Academic Press.
- Nagata, T., Arai, Y., & Momose, K. (1963). Secular variation of the geomagnetic total force during the last 5000 years. *Journal of Geophysical Research*, 68(18), 5277–5281. <https://doi.org/10.1029/j.2156-2202.1963.tb00005.x>
- Ogg, J. G. (2020). Geomagnetic polarity time scale. In F. M. Gradstein, J. G. Ogg, M. D. Schmitz, & G. M. Ogg (Eds.), *Geologic time scale 2020* (pp. 159–192).
- Paterson, G. A., Tauxe, L., Biggin, A. J., Shaar, R., & Jonestrask, L. C. (2014). On improving the selection of Thellier-type paleointensity data. *Geochemistry, Geophysics, Geosystems*, 15(4), 1180–1192. <https://doi.org/10.1002/2013GC005135>
- Perrin, M., & Shcherbakov, V. P. (1997). Paleointensity of the Earth's magnetic field for the past 400 Ma: Evidence for a dipole structure during the Mesozoic low. *Journal of Geomagnetism and Geoelectricity*, 49(4), 601–614. <https://doi.org/10.5636/jgg.49.601>
- Riisager, P., & Riisager, J. (2001). Detecting multidomain magnetic grains in Thellier paleointensity experiments. *Physics of the Earth and Planetary Interiors*, 125(1–4), 111–117. [https://doi.org/10.1016/S0031-9201\(01\)00236-9](https://doi.org/10.1016/S0031-9201(01)00236-9)
- Santos, C. N., & Tauxe, L. (2019). Investigating the accuracy, precision, and cooling rate dependence of laboratory-acquired thermal remanences during paleointensity experiments. *Geochemistry, Geophysics, Geosystems*, 20(1), 383–397. <https://doi.org/10.1029/2018GC007946>

- Selkin, P. A., & Tauxe, L. (2000). Long-term variations in palaeointensity. *Philosophical Transactions of the Royal Society of London, Series A*, 358(1768), 1065–1088. <https://doi.org/10.1098/rsta.2000.0574>
- Shcherbakov, V. P., Lhuillier, F., Gribov, S. K., Tselmovich, V. A., & Aphinogenova, N. A. (2024). Potential bias in volcanic paleomagnetic records due to superimposed chemical remanent magnetization. *Geophysical Research Letters*, 51(12), e2024GL109630. <https://doi.org/10.1029/2024gl109630>
- Shcherbakov, V. P., Lhuillier, F., & Sycheva, N. K. (2021). Exact analytical solutions for kinetic equations describing thermochemical remanence acquisition for single-domain grains: Implications for absolute paleointensity determinations. *Journal of Geophysical Research: Solid Earth*, 126(5), e2020JB021536. <https://doi.org/10.1029/2020jb021536>
- Shcherbakov, V. P., Sycheva, N. K., & Lamash, B. E. (1996). Monte Carlo modelling of TRM and CRM acquisition and comparison of their properties in an ensemble of interacting SD grains. *Geophysical Research Letters*, 23(20), 2827–2830. <https://doi.org/10.1029/96GL01999>
- Shcherbakova, V. V., Bakhmutov, V. G., Shcherbakov, V. P., Zhidkov, G. V., & Shpyra, V. V. (2012). Palaeointensity and palaeomagnetic study of Cretaceous and Palaeocene rocks from western Antarctica. *Geophysical Journal International*, 189(1), 204–228. <https://doi.org/10.1111/j.1365-246X.2012.05357.x>
- Smirnov, A. V., & Tarduno, J. A. (2003). Magnetic hysteresis monitoring of Cretaceous submarine basaltic glass during Thellier paleointensity experiments: Evidence for alteration and attendant low field bias. *Earth and Planetary Science Letters*, 206(3), 571–585. [https://doi.org/10.1016/S0012-821X\(02\)01123-8](https://doi.org/10.1016/S0012-821X(02)01123-8)
- Tarduno, J. A., Cottrell, R. D., & Smirnov, A. V. (2001). High geomagnetic intensity during the mid-Cretaceous from Thellier analyses of single plagioclase crystals. *Science*, 291(5509), 1779–1783. <https://doi.org/10.1126/science.1057519>
- Tarduno, J. A., Cottrell, R. D., & Smirnov, A. V. (2002). The Cretaceous superchron geodynamo: Observations near the tangent cylinder. *Proceedings of the National Academy of Sciences of the United States of America*, 99(22), 14020–14025. <https://doi.org/10.1073/pnas.222373499>
- Tarduno, J. A., Cottrell, R. D., & Smirnov, A. V. (2006). The paleomagnetism of single silicate crystals: Recording geomagnetic field strength during mixed polarity intervals, superchrons, and inner core growth. *Reviews of Geophysics*, 44(1), RG1002. <https://doi.org/10.1029/2005RG000189>
- Tauxe, L., & Hartl, P. (1997). 11 million years of Oligocene geomagnetic field behaviour. *Geophysical Journal International*, 128(1), 217–229. <https://doi.org/10.1111/j.1365-246X.1997.tb04082.x>
- Tauxe, L., Heslop, D., & Gilder, S. A. (2024). Assessing paleosecular variation averaging and correcting paleomagnetic inclination shallowing. *Journal of Geophysical Research: Solid Earth*, 129(8), e2024JB029502. <https://doi.org/10.1029/2024jb029502>
- Tauxe, L., Shaar, R., Jonestrask, L., Swanson-Hysell, N. L., Minnett, R., Koppers, A. A. P., et al. (2016). PmagPy: Software package for paleomagnetic data analysis and a bridge to the magnetism information consortium (MagIC) database. *Geochemistry, Geophysics, Geosystems*, 17(6), 2450–2463. <https://doi.org/10.1002/2016gc006307>
- Tauxe, L., & Staudigel, H. (2004). Strength of the geomagnetic field in the Cretaceous normal superchron: New data from submarine basaltic glass of the Troodos Ophiolite. *Geochemistry, Geophysics, Geosystems*, 5(2), Q02H06. <https://doi.org/10.1029/2003GC000635>
- Thellier, E., & Thellier, O. (1959). Sur l'intensité du champ magnétique terrestre dans le passé historique et géologique. *Annales de Géophysique*, 15(3), 285–376.
- Wack, M. R., & Gilder, S. A. (2012). The SushiBar: An automated system for paleomagnetic investigations. *Geochemistry, Geophysics, Geosystems*, 13(3), Q12Z38. <https://doi.org/10.1029/2011GC003985>
- Xu, S., & Dunlop, D. J. (2004). Thellier paleointensity theory and experiments for multidomain grains. *Journal of Geophysical Research*, 109(B7), B07103. <https://doi.org/10.1029/2004jb003024>
- Zhang, D., Yan, M., Song, C., Zhang, W., Fang, X., & Li, B. (2021). Frequent polarity reversals in the Cretaceous normal superchron. *Geophysical Research Letters*, 48(5), e2020GL091501. <https://doi.org/10.1029/2020gl091501>
- Zhu, R., Pan, Y., He, H., Qin, H., & Ren, S. (2008). Palaeomagnetism and ⁴⁰Ar/³⁹Ar age from a Cretaceous volcanic sequence, Inner Mongolia, China: Implications for the field variation during the Cretaceous normal superchron. *Physics of the Earth and Planetary Interiors*, 169(1–4), 59–75. <https://doi.org/10.1016/j.pepi.2008.07.025>
- Zhu, R., Pan, Y., & Shi, R. (2002). New Cretaceous palaeointensity data and the constraints on geodynamics. *Science in China (Series D)*, 45(10), 1–8. <https://doi.org/10.1360/02yd9092>

References From the Supporting Information

- Day, R., Fuller, M. D., & Schmidt, V. A. (1977). Hysteresis properties of titanomagnetites: Grain-size and compositional dependence. *Physics of the Earth and Planetary Interiors*, 13(4), 260–267. [https://doi.org/10.1016/0031-9201\(77\)90108-X](https://doi.org/10.1016/0031-9201(77)90108-X)
- Néel, L. (1955). Some theoretical aspects of rock-magnetism. *Advances in Physics*, 4(14), 191–243. <https://doi.org/10.1080/00018735500101204>
- Wang, D., & Van der Voo, R. (2004). The hysteresis properties of multidomain magnetite and titanomagnetite/titanomaghemite in mid-ocean ridge basalts. *Earth and Planetary Science Letters*, 220(1–2), 175–184. [https://doi.org/10.1016/s0012-821x\(04\)00052-4](https://doi.org/10.1016/s0012-821x(04)00052-4)